



Soft robotics informs how an early echinoderm moved

Richard Desatnik^{a,1} , Zach J. Patterson^{a,b,1} , Przemysław Gorzelak^c , Samuel Zamora^d , Philip LeDuc^{a,e,f,g,2}, and Carmel Majidi^{a,g,h,2}

Edited by John Rogers, Northwestern University, Evanston, IL; received April 24, 2023; accepted August 3, 2023

The transition from sessile suspension to active mobile detritus feeding in early echinoderms (c.a. 500 Mya) required sophisticated locomotion strategies. However, understanding locomotion adopted by extinct animals in the absence of trace fossils and modern analogues is extremely challenging. Here, we develop a biomimetic soft robot testbed with accompanying computational simulation to understand fundamental principles of locomotion in one of the most enigmatic mobile groups of early stalked echinoderms—pleurocystitids. We show that these Paleozoic echinoderms were likely able to move over the sea bottom by means of a muscular stem that pushed the animal forward (anteriorly). We also demonstrate that wide, sweeping gaits could have been the most effective for these echinoderms and that increasing stem length might have significantly increased velocity with minimal additional energy cost. The overall approach followed here, which we call “Paleobionics,” is a nascent but rapidly developing research agenda in which robots are designed based on extinct organisms to generate insights in engineering and evolution.

soft robotics | Paleobionics | pleurocystitids | paleontology | locomotion

Biologically inspired robots have often been used as research tools to better understand the behavior and biomechanics of their natural animal counterparts including snakes, lizards, sea turtles, and salamanders (1–5). Whereas this line of investigation has been useful, studies that use robots to explore extinct organisms have only just begun to emerge (5). Extinct organisms are a fascinating direction because the great morphological diversity in the animal kingdom that inspires robot design today is just a small fraction of all the body plans that have existed throughout history (6). Despite the promise of such opportunities, learning from extinct organisms has many challenges because what is known about them has to be pieced together from diverse information including from fossils and modern analogues. Bioinspired robots based on fossils have the potential to inform how these extinct organisms may have behaved and help reveal the biomechanical factors that drove their evolution. However, fossils are often difficult to use in robotics because preservation and interpretations impose constraints on producing accurate models.

Despite these limitations, paleontologists and roboticists have started creating artificial organisms that closely mimic extinct animals (7). These robots allow the testing of a variety of hypotheses including morphology, locomotion, and evolution. In these previous studies, researchers have developed robots to study extinct land-dwelling and semiaquatic vertebrates (5, 7). However, for these extinct organisms, researchers were able to draw on knowledge of analogous extant species and/or utilize fossilized trackways to inform their analysis. Moreover, they constructed robot testbeds using conventional robotic hardware with piecewise rigid components for the motors and linkage systems, which are very useful for some mimetic systems but have limitations. Whereas these approaches are useful for studying vertebrates, such materials and hardware architectures lack the mechanical compliance and deformability needed to study more flexible invertebrates. In this respect, the field of soft robotics (8–11) can provide unique advantages and insight into the study of invertebrates and other organisms with compliant and continuously deformable appendages.

The recent emergence of soft robotics has introduced new opportunities to model a much broader range of natural organisms, both modern and extinct (8, 9). Among the wide variety of flexible invertebrates in nature, echinoderms—the group of animals that include modern sea urchins and starfish, among others—stand out as particularly influential on the foundational principles and design of bioinspired soft robotic materials and systems. The corresponding robotic and material systems that have been investigated range from stiffness-tuning polymer nanocomposites inspired by the sea cucumber (12) and starfish-inspired robotic tube feet (13) to recent systems-level implementations of fully untethered soft robots based on the morphology of brittle stars (14, 15). Moreover, echinoderms have a rich evolutionary history, with a fossil record that extends back to the Cambrian Period (520 Mya). During the early Paleozoic Era, they showed a wide

Significance

We use soft robotics to replicate an extinct echinoderm from the Paleozoic Era and examine its biomechanics and locomotion in order to better understand the natural selection that this ancient organism experienced.

Specifically, we investigate the pleurocystitid, a member of the Rhombifera class of echinoderms that existed ca. 450 Mya and was among the first echinoderms capable of locomotion using a muscular stem. We develop a soft robotic representation and computer simulation that captures the pleurocystitid morphology and mechanics, including the compliance and flexibility of its muscular stem. This rhombiferan robot, which we call “Rhombot,” represents an early step to advance a nascent field we call “Paleobionics,” which aims to create robots based on paleontological evidence.

Author contributions: R.D., Z.J.P., P.G., S.Z., P.L., and C.M. designed research; R.D., Z.J.P., P.G., S.Z., P.L., and C.M. performed research; R.D. and Z.J.P. analyzed data; and R.D., Z.J.P., P.G., S.Z., P.L., and C.M. wrote the paper.

The authors declare no competing interest.

This article is a PNAS Direct Submission.

Copyright © 2023 the Author(s). Published by PNAS. This open access article is distributed under Creative Commons Attribution-NonCommercial-NoDerivatives License 4.0 (CC BY-NC-ND).

¹R.D. and Z.J.P. contributed equally to this work.

²To whom correspondence may be addressed. Email: prl@andrew.cmu.edu or cmajidi@andrew.cmu.edu.

This article contains supporting information online at <https://www.pnas.org/lookup/suppl/doi:10.1073/pnas.2306580120/-DCSupplemental>.

Published November 6, 2023.

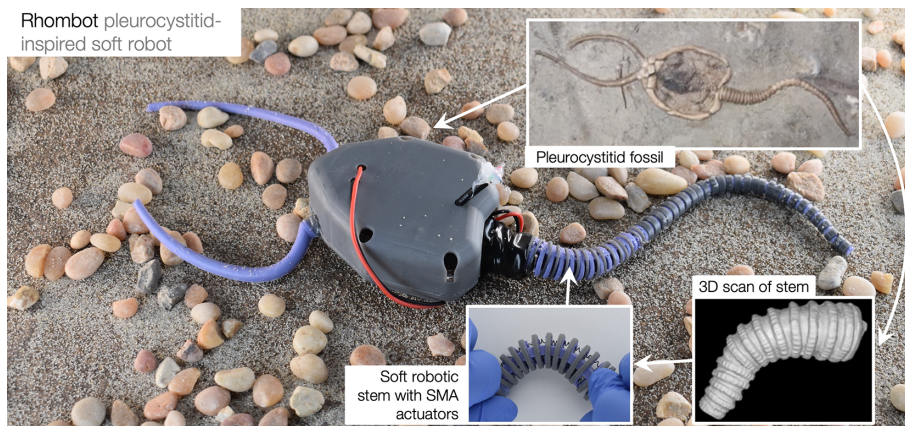


Fig. 1. “Rhombot” rhombiferan robot based on morphology of the pleurocystitid. The stem is composed of a soft elastomer embedded with shape memory alloy (SMA) muscle wire for flexural actuation. The soft robot stem is designed based on 3D scans from pleurocystitid fossils.

range of body plans and were much more diverse than they are today (16), which makes them ideally suited for exploring the biomechanics of extinct organisms using robotics—an approach that we term “Paleobionics.”

In this work, we use soft robotic testbeds and simulation tools to study the biomechanics of Paleozoic pleurocystitids. The robot, which we call Rhombot, named after the extinct Rhombifera class, uses a combination of 3D-printed elements and elastomers to mimic the skeleton-like columnal structure of the pleurocystitid stem (Fig. 1). We used fossil evidence to guide our simulation and design to determine the most meaningful test configurations. The robot is composed of a hard body, called the theca, and a flexible stem that contains shape memory alloy (SMA) artificial muscle for actuation. We utilized SMA since they are mechanically compliant, have a high work density, can be activated through electrical stimulation with minimal external electronics, and can be actuated relatively quickly when arranged antagonistically (17). [Movies S1](#) and [S2](#) show tethered and untethered versions of the SMA-powered Rhombot moving on sandy and textured surfaces, respectively.

Pleurocystites is an extinct blastozoan echinoderm genus belonging to Pleurocystidae known from the Ordovician to Devonian Periods and which are thought to have been mobile in epibenthic conditions, i.e., on the seabed and/or sediment surface (Fig. 2 A and B) (18, 19). These echinoderms were among the first capable of locomotion with the aid of a muscular stem. This innovation, combined with development of two feeding appendages (brachioles), thecal flattening, and enlargement of the periproct, likely gave them an advantage at the water-sediment interface (detritivorous) when exploring for food rather than alternative methods such as suspension feeding (suspensivores) (20, 21). However, their mode of locomotion remains uncertain, and understanding how pleurocystitids moved is especially challenging due to the lack of a modern analogue. Wagging, sweeping, sculling, or sinusoidal movements of the stem, and even swimming like a tadpole have been suggested by several researchers, but these remain untested (22–24). To explore these questions, we developed an experimental and computational pipeline to understand locomotion without relying on reference to an extant species or fossil trackways. This pipeline includes fossil analysis (Fig. 2 C–E), gait discovery using trajectory optimization in simulation (Fig. 2 F–H), and experiments with a biomimetic robot (Fig. 2 I and J).

Using this simulation and robot pipeline, we show that pleurocystitids likely moved forward (anteriorly, i.e., brachiole-first)

due to large performance advantages over stem-first (dragging the theca behind) locomotion. Second, we use the simulation and experimental robot testbed to study how variations in the length of the stem and the parameters of the gait will affect speed and efficiency. Based on the fossil evidence that pleurocystitids developed longer stems through their ontogeny and possibly also in evolutionary history (24, 26), we hypothesize that longer stems will result in more effective locomotion.

We first examine the performance of a pleurocystitid-like body plan in silico. Despite the simple appearance of the animal morphology (Fig. 3A), simulating any potential locomotion is nontrivial due to the contact-rich environment of the sea bottom. To address this, we use the differentiable Dojo physics engine, which incorporates physically realistic discrete contact (i.e., no penalty methods, as in the case of other simulators (27) and conical friction models into a time-stepping rigid body simulator (28). Referring to Fig. 3B, the pleurocystitid body plan is specified as a single rigid disc, simulating the theca, attached to a chain of rigid links that simulate the stem. Because there is no specific direct evidence for how the stem was used in locomotion, we needed to identify potential gaits. As in refs. 29 and 30, we found trajectory optimization performed with a dynamic simulator to be useful for this purpose, allowing us to find gaits that are optimal for various body plans. Critically, if we use a shooting trajectory optimization algorithm such as the Iterative Linear Quadratic Regulator (iLQR), we do not need to supply a sequence of contact modes. All that is required is a dynamically feasible input trajectory that can be achieved by an arbitrary forward dynamics simulation. As long as the potential gaits for a given body plan have clear local minima, iLQR algorithms can find these even when the initial guess is far from a minimum (31). In the context of paleontology, this means that we do not require foreknowledge of the likely gaits of a given animal because we can generate likely gaits as long as we have a body plan, unlike with collocation methods used previously for similar purposes (29, 30). With an open-ended specification of the cost function, iLQR searches a large space for local minima and spontaneously generates coherent behaviors.

Snapshots from videos of the simulation performed in Dojo ([Movie S3](#)) are shown in Fig. 3C. When using the simulation to identify potential gaits, we focus primarily on locomotion parallel to the axis of the stem, which is the most likely axis for periodic motions due to symmetry. While it has been proposed that pleurocystitids likely moved brachioles-first (24), echinoderms in general move in a number of different ways and may have

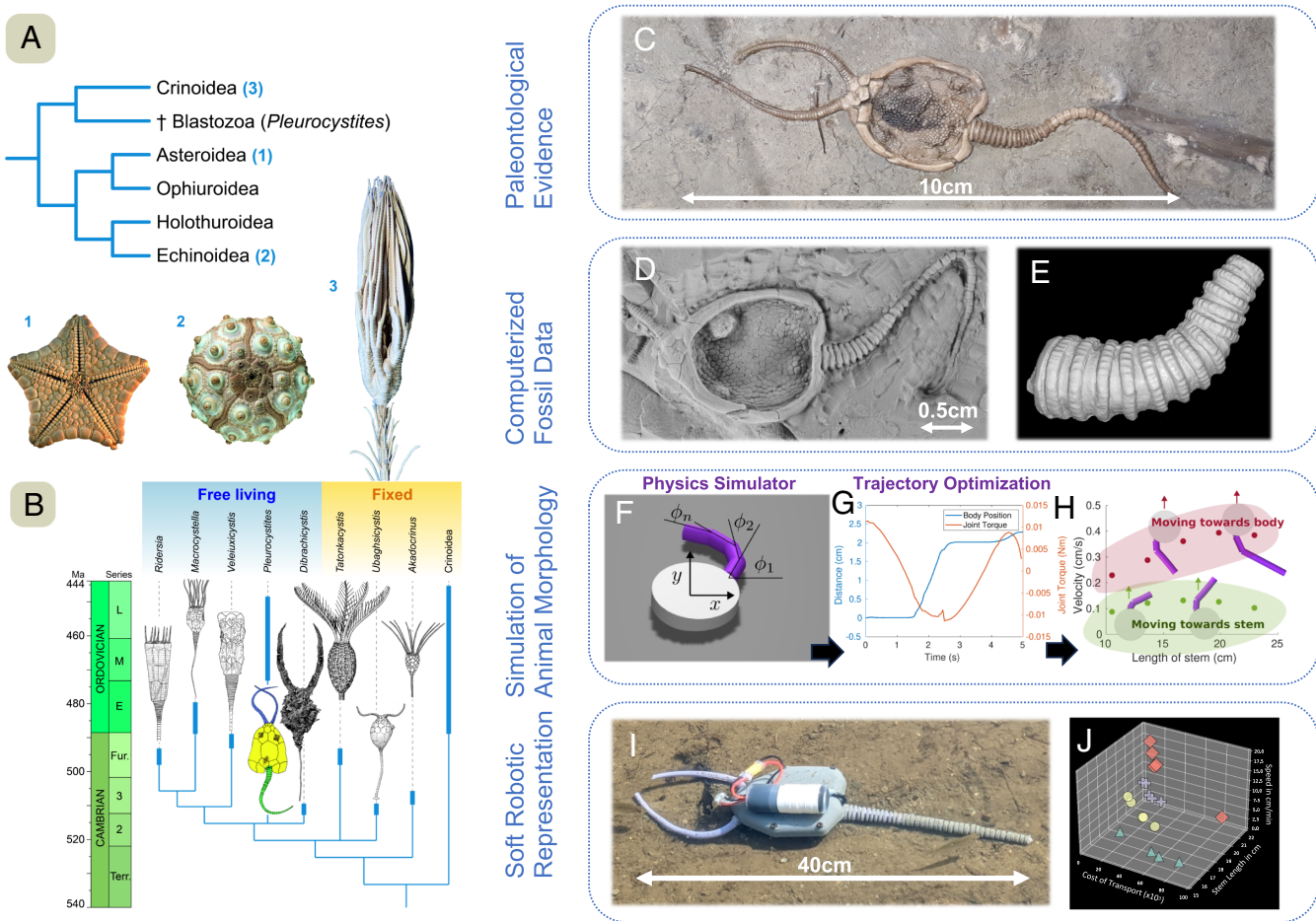


Fig. 2. Soft robotics engineering the movement of early echinoderms. (A) Phylogenetic position of modern echinoderms [after (25)], including the extinct blastozoans as a sister group of crinoids. (B) Phylogenetic tree of the earliest blastozoans with the position of *Pleurocystites* shown in yellow (18). Free-living forms derive from a sessile, permanently fixed blastozoans. (C and D) Pleurocystitid specimens from the lower Katian (Upper Ordovician) of Brechin, Ontario, Canada; (E) Tomographic reconstruction of a proximal stem. (F) Differentiable discrete mechanics simulation; (G) Optimized trajectory from iLQR; (H) Simulation data of direction of motion for various morphologies; (I) Rhombot, soft robotic representation of the pleurocystitid untethered in a local pond; (J) Gait analysis data of the pleurocystitid robot using a rigid stem and wide sweeping gait.

multiple gaits (32). We looked at several potential gaits including utilization of a fully actuated stem to perform sweeping and sinusoidal motions and utilization of the proximal stem to perform sweeping motions. Fig. 3D shows velocity and cost of transport for these trials, along with snapshots corresponding to each case. In general, sweeping gaits were more effective than sinusoidal ones, and the simulator always moves faster in a brachioles-first direction. Using a fully actuated stem can increase the velocity but also tends to increase cost of transport. To get a qualitative sense of these gaits, we provide examples in Movie S3, selected snapshots of which are shown in Fig. 3E. Because brachioles-first motion was significantly more effective in silico, we assume brachioles-first locomotion for the rest of the analysis.

After determining the more likely direction of motion, the corresponding optimal gait was tested with several body plans of varying stem length (Fig. 3F). We note that in general, velocity increases with respect to stem length until the stem is about 4 times the length of the theca (5 cm in the simulation). The same observations hold when generating a new optimal gait for each stem length (Fig. 3G). We also examine the effect of varying stiffness and sweep amplitude in simulation (SI Appendix, Figs. S3 and S4). Note that both iLQR and the Dojo simulator are deterministic and thus the numerical results reported here are as well.

Informed by the preceding analysis in simulation, we next develop similar experiments on a soft robotic prototype. To create the biomimetic pleurocystitid robot, Rhombot, we used a design and fabrication pipeline developed for creating flexible and/or soft robots (15, 33–35). To create a mimetic representation, we referenced the 3D scans of stem discussed previously along with Brower's anatomical metrics (24). Because there are no modern analogues to the pleurocystitid, having high-quality renderings of the fossils was critical in capturing a morphological counterpart to the animal. The Rhombot is 161 g and 41.7 cm in the longest stem configuration and 147 g and 36.5 cm long in the shortest stem configuration. The size of the robot is four times larger than the fossil size due to size constraints of the SMA hardware. Based on the literature, muscles were most concentrated in the proximal part of the pleurocystitid stem (24, 36). Therefore, the stem of the Rhombot is fabricated in two parts: the actuated proximal stem and the unactuated distal stem. To actuate the proximal portion, two antagonist coils of nickel–titanium (nitinol) shape memory alloy are placed within the stem. This represents one of the major assumptions of the robot model because we know that pleurocystitid had muscles between each adjacent proximal columnal. By reducing them to two antagonistic actuators, we implicitly assume that pleurocystitid used a high degree of muscle coordination along its stem to maximize exerted loads

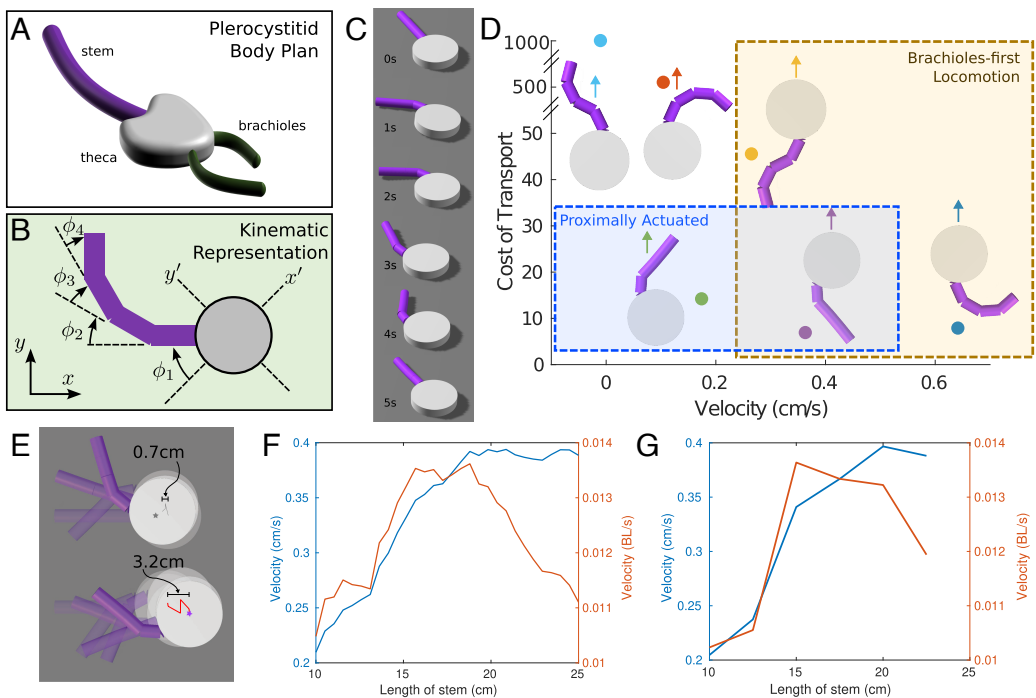


Fig. 3. Trajectory optimization results for the pleurocystitid body plan. (A) Rendering of the pleurocystitid body plan showing critical elements. (B) Kinematic representation used for the idealized pleurocystitids in simulation. (C) Snapshots of the brachioles-first gait (which is quite similar in character to the stem-first gait). (D) Comparison of optimized gaits for several configurations while attempting to move in either brachioles-first or stem-first directions. Configurations include a fully actuated stem (blue, yellow, light blue, and orange) and a proximally actuated stem (purple and green). (E) Comparison of optimal gait for stem-first (Top) and brachioles-first (Bottom) motion. The trials occurred over the same amount of time, and thus, the displacements reflect average velocity. (F) Velocity for various stem lengths based on gait depicted in C. (G) Velocity of optimal gaits optimized for each stem length.

during locomotion—an assumption backed up by results from the simulator. This approach was a balance between what is known about these extinct organisms and the technology we selected to mimic the structures of the organisms. We used flexible elastomers to mimic soft tissues within the stem and brachioles and 3D-printed components to emulate the rigid elements of the pleurocystitid (e.g., the columnals and the theca). The proximal stem contains 15 rigid cylindrical rings running along its length to mimic the columnals within the pleurocystitid stem. The distal stem in the Rhombot is comprised of 27 rigid, barrel-shaped columnals along the length and can be fabricated in a softer or stiffer configuration. The rigid theca both mimics the corresponding structure of the actual animal and serves as waterproof housing for the microcontroller. The complete structure of a fully untethered Rhombot with on-board battery can be seen in Fig. 2E, and a video of untethered locomotion is shown in Movie S2.

Because pleurocystitids are preserved in a number of different stem configurations, i.e., with straight or curved stems of various length and showing either a single or compound bends of various sweep amplitudes (37–40), we performed a series of experiments with different configurations (stem stiffness: stiff and flexible; sweep amplitude: wide and narrow; and stem length: four levels). The tethered Rhombot with a flexible stem can be seen in Fig. 4A. A full parameter sweep across this space results in 16 configurations. We used an aquarium testbed outfitted with fiducial markers to track the Rhombot’s position with respect to the world frame (SI Appendix, Fig. S6). To compare different trials, we recorded body length-scaled velocity and cost of transport (COT). A representative trial showing motion of the robot is presented in Fig. 4B and comparisons are also shown in Movie S4. Regardless of body morphology or actuation

parameters, the robot consistently moved in the brachioles-first direction. This evidence was gathered independently of the simulation and thus supports the additional benefit of brachioles-first locomotion for this body plan. Wide sweeps also, intuitively, produced much faster motion than narrow sweeps. This effect became more prominent as the stem length increased. Wide sweeping is 247 and 91 times faster than narrow sweeping for the longest stiff (Fig. 4C) and flexible (Fig. 4D) stems, respectively. Although wide sweeps consumed more energy, locomotion was still more efficient due to the large difference in velocity (Fig. 4E and F). Finally, when we alter the stem length, there are notable changes in the Rhombot speed. In particular, we find that as the stem length increases from 16.1 cm to 21.5 cm, the relative speed increases dramatically from 2.5 cm/min to 12 cm/min in the stiff configuration (Fig. 4C). This increase does not come with a significant difference in COT (Fig. 4E).

We note that, while we report velocity in the above results, we do not make specific predictions about the velocity of pleurocystitids. The study above is aimed at understanding the basic features of pleurocystitid locomotion. To produce a rigorous prediction of the velocity, we would need to take into account a number of effects such as scaling, environment, and actuation methodology. It is noteworthy, however, that the locomotion speeds of our robot are within the ranges of similarly sized modern isocrinids, which are members of the same clade of animals (Peltatozoa) (41). Admittedly, the mode of locomotion of isocrinids is different as they crawl with the aid of muscular arms. Unfortunately, the morphology of *Pleurocystites* is so disparate that direct comparison of locomotion with other echinoderm members is unlikely, as none of the modern relatives use the stem to move.

As seen in the simulations (Fig. 3) and soft robotic experiments (Fig. 4), there is a clear trend toward an increase in speed

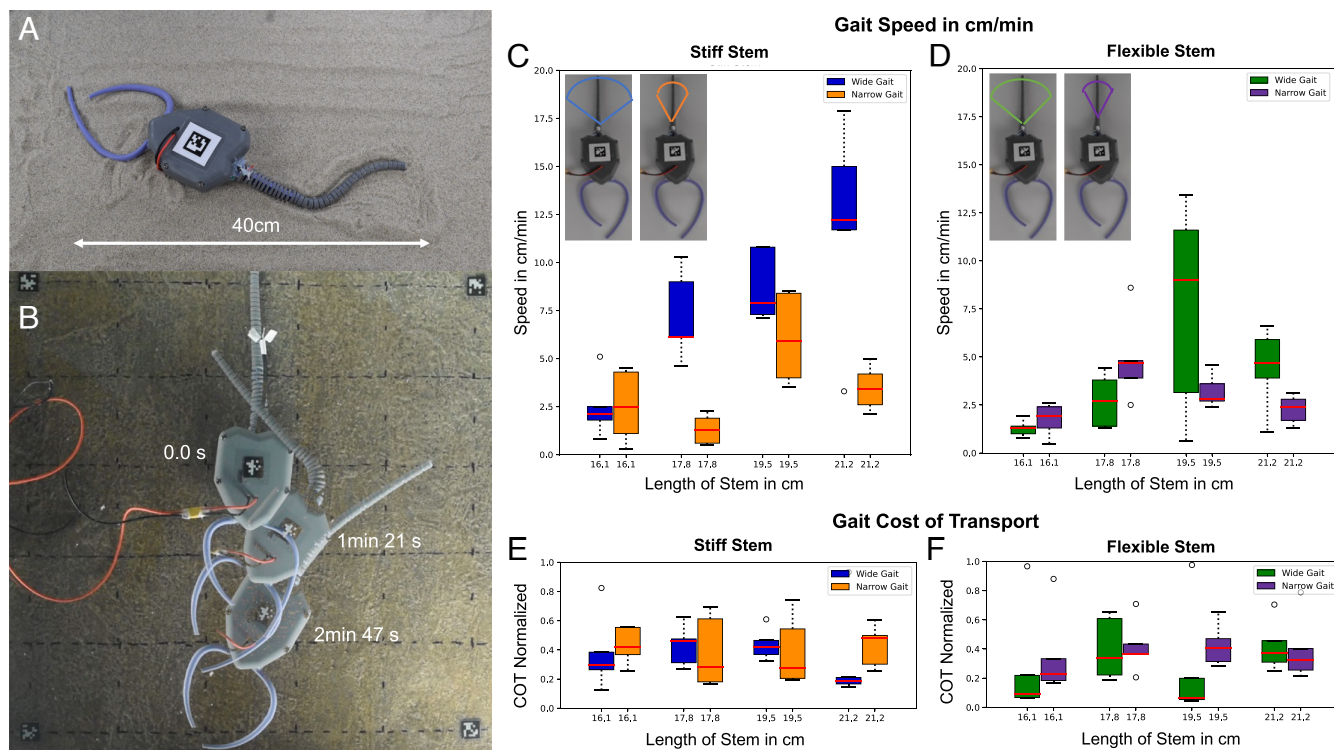


Fig. 4. Gait analysis of Rhombot with different stem sizes, sculling width, and distal stem flexibility. *(A)* Image of the robot showing its size scale. *(B)* Image of the Rhombot at different timesteps as it moves along the aquarium bed. *(C)* Graph of the differences in speed of the stiff stem in cm/min with a wide and narrow sweeping gait. *(D)* Graph of the speed of the Rhombot in the flexible stem configuration with a wide and narrow gait. *(E)* The normalized cost of transport (COT) measurements of the stiff stem layout. *(F)* The normalized COT measurements of the flexible stem.

with increasing stem length, although where this trend reverses depends on the stem characteristics. Notably, this increase does not come with a drop-off in locomotion efficiency. This finding indicates that there may have been an advantage in having a longer stem. Indeed, for some pleurocystitid species, the stem length/the cal length ratio can be as great as 3 in larger individuals (24). This is consistent with the fact that the larger-bodied adults are expected to ingest more organic detritus to meet their energetic requirements. Interestingly, although pleurocystitids are commonly incompletely preserved (i.e., they typically lack the distal-most part of the stem) and their fossil record is temporally biased, the most geologically recent (Devonian) pleurocystitids possessed somewhat longer stems. More specifically, their stem is composed of up to approximately 20 inner and outer pairs of proximal columnals and up to approximately 80 barrel-shaped columnals (38). Their maximum stem length/the cal length ratio (at least 3.4)(26), appears to be higher than those observed in the geologically older (Ordovician) pleurocystitid genera (i.e., *Amecystis* (~1.8) (20), *Plethoschisma* (~2.6) (19), *Deltacystis* (~2.8) (23), and *Pleurocystites* (~3) (24)).

The results from the simulation and experimental studies with Rhombot suggest that the stem length/the cal length ratio in some pleurocystitid taxa appears to be near optimal (~3) in terms of locomotion velocity and that the ontogenetic and evolutionary pressure to select for this trait arises from fundamental principles of locomotion. Based on the sweep amplitude data, we are also led to infer that pleurocystitids likely used large sweeping motions of the stem rather than smaller oscillatory amplitudes to locomote. In our experiments, a stiff distal stem generated a faster and more efficient gait than lower stiffness stems in most circumstances. This implies that maintaining stem stiffness would have been advantageous during locomotion.

We conjecture that the observed computational and experimental results are related to findings from geometric mechanics for drag-dominated systems. Such models suggest that, up to a point, larger changes in the state variables (e.g., bend angles) over the cycle will produce faster periodic gaits. In the geometric mechanics literature, the fastest gates enclose the largest sign definite regions of the local connection vector field (42, 43). These theories can be considered applicable to our system when it is in contact with the substrate because friction acts like drag (at low Reynolds numbers) from a dynamical systems perspective.

In closing, we created a soft robotics approach to gain insights into the locomotion and evolution of the extinct pleurocystitids. By designing the testbed based on the shape and modes of deformation inferred from the paleontological record, we were able to perform experiments and simulations using a robot representation of an extinct echinoderm with no modern analogs or fossil trackways as reference. Leveraging a principled robotic reconstruction of the organism along with shooting trajectory optimization algorithms and differentiable computational modeling, we generated insights into the influence of morphology and gait on the direction, speed, and energetic efficiency of locomotion.

Our results are strongly suggestive that: 1) pleurocystitids moved slowly in the theca-first direction; 2) in order to move faster, they needed to use large sweeping gaits rather than smaller, more rapid oscillations; 3) given this locomotion style, it is better to have a long stem than a short one, and the fossil record shows an evolutionary trend in this direction. Although our research was focused on understanding locomotion style in extinct echinoderms that have puzzled paleontologists for decades (namely pleurocystitids), the insights gained from our simulation and experiments may be potentially used to

better understand terrestrial axially driven locomotion of some tailed species (44, 45). Finally, although no extant organism is comparable to pleurocystitids, they provide a unique way to investigate robot design based on extinct morphologies with no modern analogue.

Methods

Pleurocystites is one of the first echinoderms capable of free motility with a muscular stem. Other blastozoans in the same clade were probably free living but fossils are poorly preserved and stereom has never been studied. Furthermore, in some of them (*Macrocytella*), respiratory structures are located all around the theca, and the axis of articulation between successive pairs of proximals is different (spirally arranged), which is more consistent with erect suspension feeding. As shown in *SI Appendix*, Fig. S1A, *Pleurocystites* was a bilaterally symmetric organism with a rigid body and three prominent appendages. The main body part containing most of the viscera, called the theca, is the arrow-shaped and flattened shell in the center. The two uneven anterior appendages are feeding appendages called brachioles (46). Although not much is known of the movement of the brachioles, they are composed of biserial brachiolars without any defined muscle areas or differentiation of the stereom and other structures normally associated with muscular articulations (a transverse ridge, aboral nerve canals, ligament pit, and intermuscular furrow) (*SI Appendix*, Fig. S1B), which suggests that they were mainly inflexible. With only ligaments in the brachiole, the movement, if any, would be relatively slower. They could bend only slightly down and inward at the base, like pincers, to feed on detritus (40). The third appendage is called the stem, which is the primary focus of our findings, and has two distinct parts, the proximal stem and distal stem. Recent evidence on stereom microstructure suggests that the stem was muscularized (*SI Appendix*, Fig. S1B) and thus was the primary appendage for locomotion (21). The proximal stem consists of several enlarged pairs of ring-like columnals and was likely the location of most of the muscle used for locomotion, while the distal stem consists of many smaller barrel-shaped columnals. Pleurocystitid locomotion was assumed to be sluggish and likely relied on the stem to propel itself forward, although how it did remains unknown (24) due to the lack of a modern analog or conclusive trace fossils. Lack of trace fossils ascribed to the activity of pleurocystitids is probably a result of the low preservation potential of their traces. More specifically, pleurocystitids commonly occur in high-density assemblages (*SI Appendix*, Fig. S2), which may indicate a gregarious habit for these echinoderms; thus, their traces are expected to have been overprinted by activities of the later ones and subsequent bioturbation activities of other organisms. Three pleurocystitid specimens preserving the proximal stem were selected to scan using a Micro-Computed Tomography Laboratory (Micro-CTscan) model VTomeX s 240 from GE Sensing & Inspections Technologies Phoenix X-Ray, from the Centro Nacional de Investigación sobre la Evolución Humana (CENIEH, Burgos, Spain). Specimens were isolated from the matrix to get more contrast. As a result, we obtained c.a. 2000 slices from each fossil specimen. To process the data, image reconstruction software SPIERSedit 3.1.0 has been used.

Simulation and Trajectory Optimization. The pleurocystitid was computationally simulated by idealizing the body as a serial, floating base robot in the simulation software, Dojo, a differentiable physics engine written in the Julia language that provides realistic gradients through contact (28). The only external force simulated in this package is contact with the substrate. Specifically, we assume that the substrate reacts with a combined normal force and tangential Coulombic friction force. We treat it as a densely packed solid that does not shift, move, or exhibit granular flow. Moreover, we treat the hydrodynamics of the surrounding fluid as negligible. We believe that this assumption is reasonable since the animal was likely slow enough that velocity-dependent hydrodynamics can be neglected (47). The important simulation parameters are the geometry of the body, the mass and density of the body, the friction coefficient, stiffness, and timestep. These values are cataloged in *SI Appendix*, Table S1.

The iLQR algorithm used is a first-order variant of the Differential Dynamic Programming (DDP) algorithm. Thus, given an initial rollout—simply a forward simulation of the dynamics—the algorithm iteratively performs a “backward

pass” to generate a new control sequence and then a “forward pass”/rollout with the new control inputs. Thus, the only inputs to the algorithm are the initial guess for the first rollout and the cost function for the optimizer. The cost function is a quadratic function of both the state—specifically the difference between the state and some reference trajectory—and the actuator torques. The reference trajectories used are intentionally sparse in order to minimize assumptions about the locomotion strategies that result (See *SI Appendix* for specific equations). Qualitatively, using this sparse structure for the reference encourages the simulated robot to move forward, stay close to the ground, and to use smooth and periodic motions.

To generate a candidate gait, we specified a simple hand-specified input to the stem to cause it to move back and forth. This was used as the initial guess for the optimizer. With a cost function that rewarded periodic behavior of the stem, penalized large actuator torques, and rewarded forward progress, iLQR was able to consistently converge to coherent gaits within one to several minutes. We repeated this process for both stem-first and brachioles-first locomotion. Because the optimal gait used to collect results for Fig. 2F was optimized for a given configuration (a stem length of 20 cm), the results obtained may be biased toward that configuration. To assess this, we performed a series of additional optimizations for additional stem lengths with the previous gait as starting information. Those results are shown in Fig. 2G.

Fabrication. All soft components in the Rhombot were injection molded using various elastomers. The brachioles and proximal stem were composed of a soft silicone rubber (Smooth-Sil 945; Smooth-On) that has a modulus of elasticity of 1,800 kPa. The stem is embedded with an antagonistic pair of shape memory alloy (SMA) coils (Flexinol, 0.015 in diameter; Dynalloy) that are stretched from their natural state when attached to the stem. The actuators contract through the process of Joule heating—when electrical current passes through the coil, the temperature of the alloy increases, the crystal structure changes from martensite to austenite, and the coils contract to their programmed state—causing the surrounding elastic stem to bend (48).

We used a Formlabs 3D printer with Grey and Grey Pro resins to create a mold for injection molding the silicone rubber stem. Smooth-Sil 945 (Smooth-On; Shore Hardness 45A) is used for the stiffer stems, and Ecoflex 30 (Smooth-On; Shore Hardness 030) is used for the softer stems. The SMA coils are inserted in the injection molded stem. To ensure an electrical connection, the ends of the SMA actuators are crimped to the power line. The robot is controlled with an Arduino Nano 33 IOT, which has an onboard NINA-W10 for (Bluetooth Low Energy) BLE communication. The electrical components are placed in the theca shell, which is waterproofed with Epoxyseal 9000 Electronic Grade Potting Epoxy Resin. The shell is directly printed with a Formlabs 3D printer using the Grey and Grey Pro resins. See *SI Appendix*, Fig. S5 for details on robot fabrication.

Characterization. To ensure uniformity between characterization and the test bed designed to study gaits, we created a characterization chamber (*SI Appendix*, Fig. S7A). This chamber mapped the duty cycles used to heat the SMA to the bend angle of the stem. Weights are used to fix the robot in place between trials. During the mapping process, the robot is operated at 11.1 V, which was used during the testing of the robot as this is the same voltage output of the lithium-ion batteries used in the untethered design. To determine the duty cycles required to move the limb to a defined angle, the duty cycle is gradually increased in increments of 4% to either the *Left* or the *Right* with a given actuation time of 4,000 ms or 3,000 ms. The angles are then recorded and mapped to the duty cycle used to generate them. The mapped data are in *SI Appendix*, Fig. S6.

Locomotion Experiments. The robot is placed in a 42-in by 42-in fish tank (*SI Appendix*, Fig. S7 D and E). To mimic a firm-ground seabed, we used Rock on a Roll, a surface used to line artificial ponds. The experiment’s goal was to have a consistent test surface that would mimic the firm-ground environments where some pleurocystitids are found; we note that pleurocystitids are found in a range of substrates, from soft to firm ground (26, 40). Four AprilTags are placed on the seabed 50 cm apart, and one AprilTag is placed on the Rhombot. A camera is placed above the fish tank and captures the overall displacement between

trials. We then use a computer vision algorithm to measure the videos of the displacement and speed of the robot during the tests. The unit of scaled speed is body lengths per second; this is an important metric for comparing locomotion of different robots and organisms as this measurement accounts for the scaling of speed with body size (49, 50).

The cost of transport is another metric used to compare the energy consumption of locomotion (50) and has been used previously to compare the gaits of underwater soft robots (51, 52). A high cost of transport indicates that a gait requires a large sum of energy to obtain the displacement covered by the gait. To measure the cost of transport, we recorded the output of the power supply to determine the power consumed during a test. Each test of the Rhombot consists of 15 gait cycles. A single gait cycle lasts for 8 s, and a full test lasts 2 min. Each configuration of stem stiffness, sweeping size, and stem length are run for five trials and are compared in Fig. 4.

Data, Materials, and Software Availability. All visual data was processed using our python script found at the Github link; All code used to characterize the Rhombot, operate the robot in the main test chamber, and code used to communicate with the robot data have been deposited in GitHub (<https://github.com/softmachineslab/pleurocystitid>) (53). All other data are included in the manuscript and/or supporting information.

- H. Marvi *et al.*, Sidewinding with minimal slip: Snake and robot ascent of sandy slopes. *Science* **346**, 224–229 (2014).
- T. Libby *et al.*, Tail-assisted pitch control in lizards, robots and dinosaurs. *Nature* **481**, 181–184 (2012).
- A. J. Ijspeert, A. Crespi, J. M. Cabelguen, Simulation and robotics studies of salamander locomotion: Applying neurobiological principles to the control of locomotion in robots. *Neuroinformatics* **3**, 171–195 (2005).
- R. Baines *et al.*, Multi-environment robotic transitions through adaptive morphogenesis. *Nature* **610**, 283–289 (2022).
- B. McInroe *et al.*, Tail use improves performance on soft substrates in models of early vertebrate land locomotors. *Science* **353**, 154–158 (2016).
- B. Deline *et al.*, Evolution of metazoan morphological disparity. *Proc. Natl. Acad. Sci. U.S.A.* **115**, E8909–E8918 (2018).
- J. A. Nyakatura *et al.*, Reverse-engineering the locomotion of a stem amniote. *Nature* **565**, 351–355 (2019).
- S. Coyle, C. Majidi, P. LeDuc, K. J. Hsia, Bio-inspired soft robotics: Material selection, actuation, and design. *Extrem. Mech. Lett.* **22**, 51–59 (2018).
- S. Kim, C. Laschi, B. Trimmer, Soft robotics: A bioinspired evolution in robotics. *Trends Biotechnol.* **31**, 287–294 (2013).
- S. I. Rich, R. J. Wood, C. Majidi, Untethered soft robotics. *Nat. Electr.* **1**, 102–112 (2018).
- D. Rus, M. T. Tolley, Design, fabrication and control of soft robots. *Nature* **521**, 467–475 (2015).
- K. Shanmuganathan, J. R. Capadona, S. J. Rowan, C. Weder, Biomimetic mechanically adaptive nanocomposites. *Progr. Polymer Sci.* **35**, 212–222 (2010).
- M. A. Bell *et al.*, Echinoderm-inspired tube feet for robust robot locomotion and adhesion. *IEEE Robot. Autom. Lett.* **3**, 2222–2228 (2018).
- Z. J. Patterson, A. P. Sabelhaus, K. Chin, T. Hellebrekers, C. Majidi, “An untethered brittle star-inspired soft robot for closed-loop underwater locomotion” in *2020 IEEE/RSJ International Conference on Intelligent Robots and Systems (IROS)* (IEEE, 2020), pp. 8758–8764.
- Z. J. Patterson, D. K. Patel, S. Bergbreiter, L. Yao, C. Majidi, A method for 3D printing and rapid prototyping of fieldable untethered soft robots. *Soft Robot.* **10**, 292–300 (2023).
- C. D. Sumrall, G. A. Wray, Ontogeny in the fossil record: Diversification of body plans and the evolution of “aberrant” symmetry in Paleozoic echinoderms. *Paleobiology* **33**, 149–163 (2007).
- X. Huang *et al.*, Shape memory materials for electrically-powered soft machines. *J. Mater. Chem. B* **8**, 4539–4551 (2020).
- S. Zamora, A. Smith, Cambrian stalked echinoderms show unexpected plasticity of arm construction. *Proc. R. Soc. B: Biol. Sci.* **279**, 293–298 (2012).
- C. D. Sumrall, J. Sprinkle, Plating and pectinirhombs of the Ordovician *Rhombiferan plethoschisma*. *J. Paleontol.* **69**, 772–778 (1995).
- R. L. Parsley, *Revision of the North American Pleurocystitida (Rhombifera-Cystoidea)* (Paleontological Research Institution, 1970).
- P. Gorzelak, S. Zamora, Understanding form and function of the stem in early flattened echinoderms (Pleurocystitids) using a microstructural approach. *PeerJ* **4**, e1820 (2016).
- C. R. Paul, “The functional morphology and mode of life of the cystoid Pleurocystites E. Billings, 1854” in *Echinoderm Biology. Symposium of the Zoological Society of London*, E. Milot, Eds. (Academic Press, 1967), vol. 20, pp. 105–123.
- J. Sprinkle, New Rhombiferan cystoids from the Middle Ordovician of Nevada. *J. Paleontol.*, 1174–1201 (1974).
- J. C. Brower, A new pleurocystitid Rhombiferan echinoderm from the Middle Ordovician Galena Group of northern Iowa and southern Minnesota. *J. Paleontol.* **73**, 129–153 (1999).
- K. Nanglu, S. R. Cole, D. F. Wright, C. Souto, Worms and gills, plates and spines: The evolutionary origins and incredible disparity of deuterostomes revealed by fossils, genes, and development. *Biol. Rev.* **98**, 316–351 (2023).
- E. Nardin, J. Bohatý, A new pleurocystitid blastozoan from the Middle Devonian of the Eifel (Germany) and its phylogenetic importance. *Acta Palaeontol. Polonica* **58**, 533–544 (2012).
- E. Todorov, T. Erez, Y. Tassa, “MuJoCo: A physics engine for model-based control” in *2012 IEEE/RSJ International Conference on Intelligent Robots and Systems* (IEEE, 2012), pp. 5026–5033.
- T. A. Howell, S. L. Clea'ch, J. Z. Kolter, M. Schwager, Z. Manchester, Dojo: A differentiable simulator for robotics. *arXiv [Preprint]* (2022). <http://arxiv.org/abs/2203.00806> (Accessed 2 December 2022).
- P. J. Bishop, A. Falisse, F. De Groote, J. R. Hutchinson, Predictive simulations of running gait reveal a critical dynamic role for the tail in bipedal dinosaur locomotion. *Sci. Adv.* **7**, eabi7348 (2021).
- D. T. Polet, J. R. Hutchinson, Estimating gaits of an ancient crocodile-line archosaur through trajectory optimization, with comparison to fossil trackways. *Front. Bioeng. Biotechnol.* **9**, 800311 (2022).
- E. Todorov, W. Li, “A generalized iterative lqg method for locally-optimal feedback control of constrained nonlinear stochastic systems” in *Proceedings of the 2005 American Control Conference, 2005* (IEEE, 2005), pp. 300–306.
- I. A. Rahman, R. P. Jefferies, W. H. Suedkamp, R. D. Smith, Ichnological insights into Mitrate Palaeobiology. *Palaeontology* **52**, 127–138 (2009).
- A. Wertz, A. P. Sabelhaus, C. Majidi, “Trajectory optimization for thermally-actuated soft planar robot limbs” in *2022 IEEE 5th International Conference on Soft Robotics (RoboSoft)* (IEEE, 2022), pp. 439–446.
- A. P. Sabelhaus, Z. J. Patterson, A. T. Wertz, C. Majidi, Safe supervisory control of soft robot actuators. *arXiv [Preprint]* (2022). <http://arxiv.org/abs/2208.01547> (Accessed 2 December 2022).
- Z. J. Patterson, A. P. Sabelhaus, C. Majidi, Robust control of a multi-axis shape memory alloy-driven soft manipulator. *IEEE Robot. Autom. Lett.* **7**, 2210–2217 (2022).
- S. K. Donovan, The improbability of a muscular crinoid column. *Lethaia* **22**, 307–315 (1989).
- F. A. Batter, *Caradocian cystidea from Girvan* (R. Grant & Son, 1913), vol. 49.
- R. V. Kesling, D. Le Vesvre, *Strataster ohioensis, a New Early Mississippian Brittle-star, and the Paleoecology of Its Community* (University of Michigan, Museum of Paleontology, 1971).
- C. R. C. Paul, British Ordovician cystoids. *Monogr. Palaeont. Soc.* **136**, 65–152 (1982).
- J. C. Brower, Paleoecology of echinoderm assemblages from the upper Ordovician (Kataian) Dunleith formation of northern Iowa and southern Minnesota. *J. Paleontol.* **87**, 16–43 (2013).
- T. K. Baumiller, C. G. Messing, Stalked crinoid locomotion, and its ecological and evolutionary implications. *Palaeontol. Elect.* **10**, 1 (2007).
- S. Ramasamy, R. L. Hatton, The geometry of optimal gaits for drag-dominated kinematic systems. *IEEE Trans. Robot.* **35**, 1014–1033 (2019).
- J. E. Avron, O. Raz, A geometric theory of swimming: Purcell's swimmer and its symmetrized cousin. *New J. Phys.* **10**, 063016 (2008).
- K. Jagannadan, T. E. Higham, Lateral movements of a massive tail influence gecko locomotion: An integrative study comparing tail restriction and autotomy. *Sci. Rep.* **7**, 1–8 (2017).
- C. Pace, A. C. Gibb, Sustained periodic terrestrial locomotion in air-breathing fishes. *J. Fish Biol.* **84**, 639–660 (2014).
- S. Zamora, C. D. Sumrall, X. J. Zhu, B. Lefebvre, A new stemmed echinoderm from the Furongian of China and the origin of Glyptocystitida (Blastozoa, Echinodermata). *Geol. Maga.* **154**, 465–475 (2017).
- S. M. Song, K. J. Waldron, *Machines that Walk: The Adaptive Suspension Vehicle* (MIT Press, 1989).
- L. C. Brinson, One-dimensional constitutive behavior of shape memory alloys: Thermomechanical derivation with non-constant material functions and redefined martensite internal variable. *J. Intell. Mater. Syst. Struct.* **4**, 229–242 (1993).
- X. Huang, K. Kumar, M. K. Jawed, Z. Ye, C. Majidi, Soft electrically actuated quadruped (SEAQ)-integrating a flex circuit board and elastomeric limbs for versatile mobility. *IEEE Rob. Autom. Lett.* **4**, 2415–2422 (2019).
- R. M. Alexander, *Principles of Animal Locomotion* (Princeton University Press, 2003).
- J. Lee *et al.*, Bioinspired soft robotic fish for wireless underwater control of gliding locomotion. *Adv. Intell. Syst.* **4**, 2100271 (2022).
- C. Christianson *et al.*, Jellyfish-inspired soft robot driven by fluid electrode dielectric organic robotic actuators. *Front. Robot. AI* **6**, 126 (2019).
- R. Desatinik *et al.*, “Simulation Code for Rhombot modeling.” GitHub. <https://github.com/softmachineslab/pleurocystitid>. Deposited 18 January 2023.

ACKNOWLEDGMENTS. This research was supported by the following grants: National GEM Consortium through the GEM Fellows Program (R.D.); National Oceanographic Partnership Program, Grant N00014-18-12843, PM: Reginald Beach (Z.J.P., C.M.); Spanish Ministry of Science, Innovation and Universities PID2021-125585NB-I00, (S.Z.); Government of Aragon project “Aragosaurus,” E18-17R (S.Z.); “Severo Ochoa” grant IGME-CSIC AECEX2021 (S.Z.); NSF grant CMMI-1946456 (P.L.); Air Force Office of Scientific Research grant FA9550-18-1-0262 (P.L.); National Institute of Health grant R21AR08105201A1; R01AG06100501A1 (P.L.). Fossil specimens analyzed in this study were collected by Joseph M. Koniecki (Michigan, USA), and we thank his collaboration. Jean-Bernard Caron and Maryam Akrami made specimens from the Royal Ontario Museum available for us.

Author affiliations: ^aMechanical Engineering, Carnegie Mellon University, Pittsburgh, PA 15213; ^bComputer Science and Artificial Intelligence Laboratory, Massachusetts Institute of Technology, Cambridge, MA 02139; ^cInstitute of Paleobiology, Polish Academy of Sciences, Warsaw 00-818, Poland; ^dInstituto Geológico y Minero de España - Consejo Superior de Investigaciones Científicas, Residencia, Campus Aula Dei, Zaragoza 50059, Spain; ^eBiological Sciences, Carnegie Mellon University, Pittsburgh, PA 15213; ^fComputational Biology, Carnegie Mellon University, Pittsburgh, PA 15213; ^gBiomedical Engineering, Carnegie Mellon University, Pittsburgh, PA 15213; and ^hRobotics Institute, Carnegie Mellon University, Pittsburgh, PA 15213